

https://doi.org/10.70917/jcc-2025-003 Article

# Numerical Optimization of Thermoelectric Heat Pump Assisted Drying System

Amir Azirul <sup>1</sup>, Adnan Ibrahim <sup>1</sup>, Nurul Syakirah Nazri <sup>1</sup>, Hasila Jarimil <sup>2</sup>, Muhammad Ammirrul Atiqi Mohd Zainuri <sup>3</sup> and Ubaidah Syafiq <sup>1,\*</sup>

- 1 Solar Energy Research Institute, Universiti Kebangsaan Malaysia, Bangi 43600, Selangor, Malaysia; p130551@siswa.ukm.edu.my (A.A.); iadnan@ukm.edu.my (A.I.); nurulsyakirah@ukm.edu.my (N.S.)
- Department of Architecture and Built Environment, The University of Nottingham, NG7 2RD, UK; hasila.harimi@ukm.edu.my
- Department of Electrical, Electronic and Systems Engineering, Faculty of Engineering and Built Environment, Universiti Kebangsaan Malaysia, Bangi 43600, Selangor, Malaysia; ammirulatiqi@ukm.edu.my;
- \* Correspondence author: ubaidahsyafiq@ukm.edu.my

Abstract: One of the methods for food preservation involves utilizing the heat from solar radiation to remove moisture, aptly known as solar drying. Different approaches in enhancing solar dryer efficiency have been made throughout the years, involving circulation refinements, mechanism improvements, and insulation enhancements. Thermoelectric heat pumps (TEHP) leverage the Peltier effect to generate temperature difference that can be integrated with solar dryer system. However, the information on design and parameters for integration is scarce and underexplored. In this work, TEHP-assisted solar drying system was designed and the ideal parameters for efficient drying rate were determined by optimizing fan position and airflow rate. The system's performance was gauged through moisture content reduction of drying loads (ginger). CFD numerical optimization was performed at the airflow rate between 0.003–0.012 m³/s, at three different fan locations. Results showed that lower airflow rate increases the accumulated heat inside the chamber, resulting in higher moisture content removal within the load, thus increasing drying rate. Even though the higher airflow showed greater reduction in H2O mass, reduction of drying chamber temperature was also observed, resulting in reduced effectiveness in moisture removal. The ideal fan position and airflow rate were determined to be at the system inlet (Fan 1) and 0.012 m³/s, respectively. The results from this work show the importance of fan position and airflow rate on a TEHP-assisted solar dryer towards its the drying rate to achieve a balance between energy consumption and effective drying.

Keywords: modelling and simulation; numerical optimization; solar drying system; thermoelectric heat pump

#### 1. Introduction

Solar energy represents a promising and sustainable renewable source to potentially address global challenges such as climate change (Rahmat et al., 2022) and food (Gomez-Casanovas et al., 2023). It is an attractive alternative source for power generation due to its abundance and environmental benefits compared to the traditional fossil fuels which are proven to pose adverse ecological impacts. A particular noteworthy representation of solar energy utilization is evident in the area of food preservation (Fernandes and Tavares, 2024). The food preservation technique through harnessing solar power illustrates an innovative approach in promoting sustainable practices in many sectors, especially with enhancing the food security in increasing shelf life, paving the way for a more sustainable future. The food preservation technique harnesses the radiation from the sun to remove moisture from food products. This technique is called solar drying, and it plays a pivotal role in diminishing food loss and waste issues in the food industry (Shamshiri et al., 2024). Solar drying can reduce greenhouse gas emissions and serve as a catalyst for economic development through employment opportunities within the food processing industry and solar energy (Amjad et al., 2023). It has been reported that the usage of solar drying techniques among industry sector has enhanced the quality of



Copyright: © 2025 by the authors

products, contributed to improving market prices, and noticeably increased income for the rural communities within the domain of the food processing industry (Herrando et al., 2023). The promising approach showcased an effective reduction in spoilage rate in the product due to the development and consequently contribute to better health benefits and nutritional value of products for consumers (Hii et al., 2019). The implementation is noticeable where it fosters economic growth and promotes healthier consumption patterns for consumers either within the rural or urban settings.

As summarized in Table 1, solar dryers can be categorized by its unique design according to its intended use such as active, passive solar dryers and open sun drying (Workineh Daksa and Neme Tolesa, 2023). Passive solar dryers use natural flow of air through a strategic system combination that is effective in regulating the airflow by manipulating wind pressure and buoyancy-driven currents within their structure to ensure optimal drying (Kherrafi et al., 2024). The system is often made from inexpensive material to ensure affordability to farmers looking for small-scale applications for drying fruits and vegetables at a temperature ~50 °C (Herrando et al., 2023). However, passive solar dryer has a slow drying rate compared to their active counterparts. Active solar dryers dry with fans to maintain a consistent controlled airflow that aids in ensuring the warm air within the drying cabinet is evenly distributed throughout the operation. The airflow mechanism ensures the product is being dried thoroughly as fast as possible to extract moisture from the product. However, this increases the energy usage of the solar dryer due to the energy it consumes to operate the fan. Nonetheless, it is important to acknowledge that the active solar dryers delve with a multitude of parameters including temperature, humidity, airflow and environmental conditions in its sophisticated design to optimize the drying process(D. Pagukuman and Wan Ibrahim, 2021). Hence, the intricate interplay of these parameters determines the effectiveness and well design of solar dryers even if the system is well monitored and affect the drying product characteristic such as moisture content and physical properties. A balance of each parameter of active solar dryer is needed to produce a quality product.

There has been a variety of studies conducted to explore the different approaches to enhance solar dryer efficiency. These endeavours mostly focused on careful implementation of refining the recirculation, improving the operational mechanism of the system and also a consideration in enhancing the insulation properties (Ekka et al., 2021). Several studies have been worked on introducing a heat pump(Herez, 2021, Jalal Abduelgader et al., 2020), phase change material (PCM)(PÁSSARO, 2022, Lim and Jeong, 2020), and geothermal energy (Jaiswal et al., 2023) as a reserve energy supply for flexible energy utilization and to reduce the dependency on direct solar radiation as a heat supply. It ensures a continuous drying of products, preventing rehydration (Deng et al., 2021). These dryers are known as hybrid solar dryers and it is developed for the purpose of overcoming the limitations of conventional solar dryers and improve overall drying efficiency of products (Zeinab et al., 2022). Rani et al. used baffles and semicircular loops in solar dryers to optimize the heat distribution and air circulation inside the drying chamber (Rani and Tripathy, 2023). Hussain et al. used a backup heater in the solar dryer that decreased the drying time by 70% (Hussain et al., 2021). There is also research that accounts for the utilization of thermoelectric heat pumps (TEHP) as a heater by using the Peltier effect for warming purposes without the need for traditional method like combustion or electric resistance heating to reduce carbon emissions and energy wastage associated with conventional heating systems. Garayo et al. presented thermoelectric heat pumps with a ventilation system for passive houses, where the heating capacity reaches 1200 W with COP ranging from 1.5-4 to improve the energy performance (Diaz de Garayo et al., 2021).

TEHP is an electronic appliance which utilizes Peltier effect to transfer heat from the thermoelectric material to the environment, intended to be used for heating (Martinez et al., 2019). Peltier effect is generated when an electric current is given to two thermoelectric materials with different electronic properties known as p-type and n-type materials (Xu et al., 2023). TEHP is an innovative and promising technology in heat pump appliances that gives many benefits such as refrigerant free, reducing moving mechanical parts, and minimum maintenance (Cheon et al., 2019). Moreover, TEHP has better temperature control compared to conventional heat pumps in transiting from heating to cooling mode, along with easier integration with photovoltaic (PV) system (Tomc et al., 2024). Fahruddin et al. presented TEHP influence on the surrounding air by analysing the changes in temperature and humidity, where it harnesses the cool side of the TEHP for the purpose of water harvesting and to reach a desired temperature of 25.6 °C, free from excess moisture with the humidity of 78% when the temperature of the surrounding air is 31 °C (Fahruddin et al., 2022). TEHP can be manufactured by a variety of structures such as the conventional thermoelectric  $\pi$ -type, thin thermoelectric, annular module and stacking (Evstatieva et al.). Most of these structures has its own advantages and disadvantages and can be seen to be used with its own condition and purposes. However, the information on design and parameters for integration is scarce and underexplored. In this work, TEHP-assisted solar drying system was designed and the ideal parameters for efficient drying rate were determined by optimizing fan position and airflow

rate. The system's performance was evaluated through moisture content reduction of drying loads (ginger).

Table 1. Different categories of solar dryer.

System Type	e	Key Contributions	Limitations/Gaps	Reference
		Inexpensive materials for small-scale drying (~50 °C).	Slow drying rate compared to active systems.	(Herrando et al., 2023)
Passive S Dryers	Solar	Natural airflow mechanism influenced by wind pressure and buoyancy.	Limited efficiency in fluctuating weather conditions; lacks detailed studies on airflow optimization.	(Kherrafi et al., 2024)
	Solar	Optimized drying using parameters like temperature, humidity, and airflow.	High energy consumption due to fan operation; challenges in balancing energy use and drying speed.	(D. Pagukuman and Wan Ibrahim, 2021)
Active Son Dryers		Introduced baffles and semicircular loops for better heat and air distribution.	Limited scalability: performance under diverse environmental conditions needs further study.	(Rani and Tripathy, 2023)
		Backup heaters reduced drying time by 70%.	Increases energy dependence, which may not be viable in remote or off-grid areas.	(Hussain et al., 2021)
	Solar	Integration of heat pumps to improve energy efficiency.	High initial cost; complexity in integrating heat pumps with solar drying systems.	(Herez, 2021, Jalal Abduelgader et al., 2020)
		PCM as a backup energy source to reduce dependency on direct solar radiation.	Limited research on PCM material degradation and long-term performance.	(PÁSSARO, 2022, Lim and Jeong, 2020)
Hybrid S Dryers		Explored geothermal energy as an alternative heat source.	High dependency on geographical feasibility; requires advanced infrastructure for deployment.	(Jaiswal et al., 2023)
		Addressed continuous drying mechanisms to prevent rehydration.	Lack of detailed analysis on energy savings and environmental impacts.	(Deng et al., 2021)
		Hybrid systems overcome	High operational complexity; difficulty	(Zeinab et al., 2022)

	conventional solar dryer limitations and enhance drying efficiency.	in standardizing hybrid designs across regions.	
	Improved drying consistency and energy utilization.	Long-term operational stability remains unclear.	(Zeinab et al., 2022)
TEHP-Based Systems	TEHPs achieved 1200 W heating capacity with COP of 1.5–4.	High cost; efficiency heavily dependent on material quality and operational conditions.	(Diaz de Garayo et al., 2021)
	Described as the Peltier effect and thermoelectric materials (p-type and n-type).	Limited adoption due to cost and lack of robust testing for durability.	(Xu et al., 2023, Martinez et al., 2019)
	Highlighted advantages like refrigerant-free operation and minimal maintenance.	TEHPs still require significant energy input, especially in large-scale applications.	(Cheon et al., 2019)
	Better temperature control and PV integration with TEHPs.	Lacks real-world application data to support integration feasibility with existing solar dryers.	(Tomc et al., 2024)
	TEHPs managed air temperature and humidity, achieving 25.6 °C and 78% humidity.	Limited studies on the environmental and energy performance under varying climatic conditions.	(Fahruddin et al., 2022)
	Various TEHP structures (π-type, thin thermoelectric, annular, and stacking).	Lack of comparative studies to identify the best structure for specific drying needs.	(Evstatieva et al.)

In this study, the potential application of TEHP in a drying system is explored. TEHP offers notable advantages over conventional heat pump dryers, unlike conventional systems that rely on refrigerants with associated environmental concerns, it is refrigerant-free, thereby reducing greenhouse gas emissions. Notably, its solid-state design eliminates the need for mechanical components such as compressors and bulky condensers, leading to reduced maintenance requirements and increased reliability. Furthermore, TEHP provides precise temperature control, enabling efficient transitions between heating and cooling modes, which is particularly beneficial for drying sensitive materials. When integrated with solar PV, TEHP system can demonstrate higher energy efficiency since it will be utilizing renewable resources, reducing operational costs, and minimizing dependence on grid electricity. This makes TEHPs particularly advantageous for off-grid applications, where access to conventional power infrastructure is limited. Additionally, the use of DC electricity in TEHPs reduces the overall cost of off-grid solar PV systems by eliminating the need for an electric inverter. The absence of moving parts further minimizes noise levels, making TEHPs particularly suitable for small-scale or indoor drying applications where space and quiet operation are critical. These features position solar-powered TEHPs as a practical and sustainable solution for efficient drying processes, especially in remote or off-grid settings.

In our research, computer modelling and simulations allow us to perform initial assessments without

the need for the device or system physically. It is a time-saving mechanism that can be employed for the purpose of predicting the output of temperature, relative humidity and airflow of a solar dryer (Wan et al., 2023). Furthermore, the simulation can be executed numerous times to find the optimal criteria that align with the solar drying system requirements. In addition, the uncertainties of such a complex system such as solar dryers can be reduced when addressed by implementing modelling and simulation techniques and may predict the best system to avoid over and under design.

To set it apart from previous studies, the present study highlights the relevant parameters in constructing a TEHPs with solar drying chamber such as airflow patterns, material properties, and moisture content to serve as a reference in expanding and optimizing the design, utilizing a heat sink and airflow pathing that may assist with TEHP configuration to increase drying rate. By placing a fan at a relevant location, we can showcase an increase in drying rate to effectively distribute heat. Through the simulation-based studies under multiple operating conditions, this study may contribute to the understanding of heat and air distribution over time in a TEHP-assisted solar drying system in identifying potential areas for future improvements. This study also demonstrates the capability of TEHP-assisted solar drying system to be integrated with a PV system, to increase overall system efficiency.

## 2. Methodology

In this study, we first design the TEHP-assisted solar drying system, which comprises a drying chamber heated by a TEHP and fully powered by a standalone solar PV system. In this preliminary investigation to validate the design concept, the TEHP-assisted solar drying system is optimized using a Multiphysics approach coupled with Computational Fluid Dynamics (CFD). The use of CFD, particularly through reliable simulation tools like ANSYS Fluent, ensures accurate modelling of complex fluid flow and heat transfer phenomena within the drying chamber. This approach enables precise predictions of airflow patterns, temperature distributions, and moisture removal efficiency, which are critical for the system's performance. The advanced numerical techniques in CFD have been extensively validated in similar drying system applications, making it a trusted methodology for design optimization. This combined approach helps design an efficient solar drying system by optimizing airflow rates for improved airflow management, ultimately reducing moisture content effectively.

### 2.1. Solar Dryer Design

The drying chamber serves as the environment where the drying process of removing moisture from the material occurs. It is designed to allow temperature and airflow to remove moisture toward the chamber outlet. The drying chamber in the TEHP-Assisted solar drying system is a rack-type drying system, with the details outlined in Table 2. This system is known for its ability to dry large quantities of materials such as chili, turmeric, and okra (Mugi and Chandramohan, 2021). In this study, the drying chamber is designed measuring  $0.5 \text{ m} \times 0.5 \text{ m} \times 1 \text{ m}$  and is constructed from aluminium. It features three shelves, referred to as the upper rack, middle rack, and lower rack. A TEHP is integrated into the drying chamber to assist the drying process. The TEHP is located below the lower rack, allowing air to move upwards through the drying chamber towards the outlet (Szpicer et al., 2023). It is worth noting here that the system integrates a simulated photovoltaic-thermoelectric-thermal (PVTET) system, where the airflow output serves as the input for the drying chamber. The air that passes through the PVTET system retains some amount of heat, enhancing the operational thermal efficiency of the TEHP-assisted solar drying system. However, the simulation of the PVTET system is currently beyond the scope of this paper, as the primary focus is on the performance of the drying chamber.

Three different fan locations in the solar drying system are modelled to facilitate the strategic distribution of airflow throughout the drying chamber, operating under conditions where the inlet relative humidity is maintained at 100%. The ginger is arranged on the three shelves within the drying chamber to ensure even heat exposure. This approach efficiently keeps heat and ensures thorough drying, producing high-quality dried ginger suitable for storage or post-processing.

The hot side temperature (Th) of the TEHP is set at 50 °C, simulating the desired heating temperature during operation. Additionally, the panel of the PVTET system is set to a temperature of 60 °C to simulate outdoor solar conditions. The airflow, heat distribution, and performance of the solar drying system are predicted using a three-dimensional solver. Based on the simulation results, the optimal fan location and airflow configuration will be identified. Transient numerical models were employed to simulate heat distribution by convection and conduction within the system, operating at different airflow rates to enhance performance. The numerical model provides insights into the interplay between heat distribution and airflow, offering data to improve system efficiency. A detailed simulation will highlight the impact of fluid parameter boundary conditions and the significance of numerical analysis in enhancing the solar drying system's performance. The overview of the model's design is illustrated in Figure 1. The aim of

this study is to analyse numerically the following key parameters:

- (i) The effectiveness of different fan positions in controlling airflow distribution in the drying chamber.
- (ii) The effect of different airflow rates on moisture removal.
- (iii) The effect of different airflow rates on temperature distribution in the TEHP-assisted solar drying system.

Table 2. Design parameters of the TEHP-assisted solar drying system.

Parameter	Description	Value/Specification
Chamber Dimensions	Length × Width × Height	0.5 m × 0.5 m × 1 m
Material	Construction material	Aluminium
Rack Type	Number of racks	3 (Upper, Middle, Lower)
Rack Dimensions	Length × Width × Height	$0.5 \times 0.5 \times 0.03 \text{ m}$
TEHP Position	Placement of thermoelectric heat pump	Below the lower rack
Th Operation	Contact with heat sink panel to transfer heat to the drying chamber air	
Cold side (T <sub>c</sub> ) Operation	Contribution to the process	Ignored
Airflow Mechanism	Air circulation through fan placement	Variable fan positions
Fan Airflow Rate Airflow rates		0.003, 0.006, 0.009, 0.012 m <sup>3</sup> /s
Temperature Setting	* I I & OL LEHP	
Relative Humidity	Inlet condition	100% RH

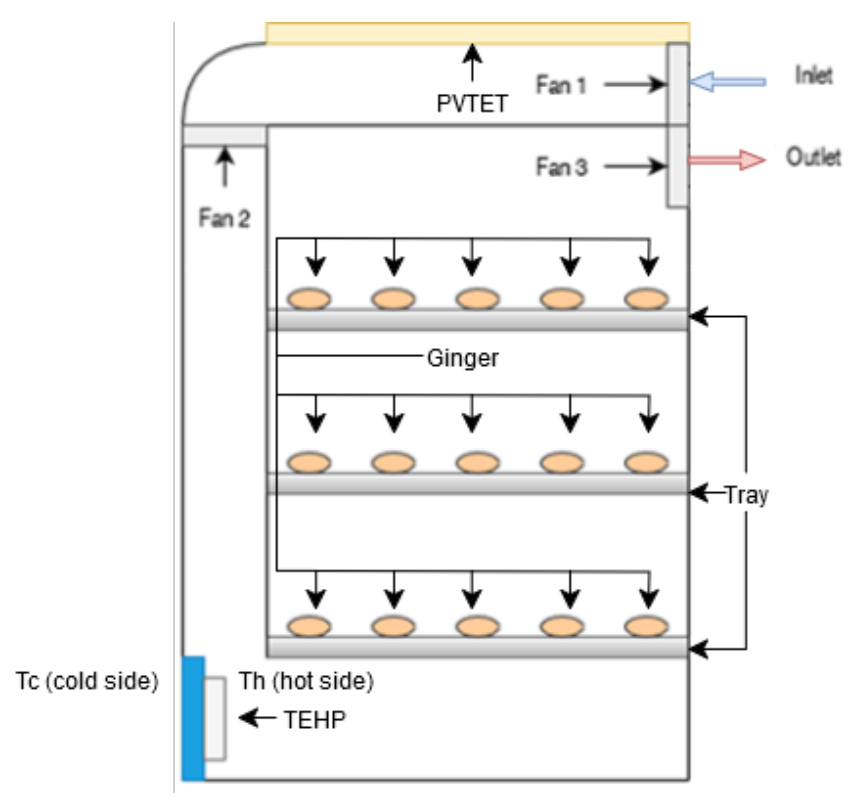


*Figure 1.* Diagram of the TEHP-assisted solar drying system with proposed fan locations used in the computational fluid dynamics (CFD) simulation.

Three fan locations are selected for the simulation: i) at the system inlet (Fan 1), ii) after passing PVTET system (Fan 2), and iii) at the system outlet (Fan 3), as shown in Figure 1. Fan 1 is located at the

system inlet to allow for active heat convection between the heat sink of the PVTET system and the air. Fan 2 is located after passing the PVTET system to allow for passive heat convection between the heat sink of the PVTET system and the air. Lastly, Fan 3 is located at the system outlet to assist with the removal of heat and humidity from inside the chamber. The airflow and fan location for the most optimal solar drying system design will be selected based on the fastest drying rate.

# 2.2. Drying Load Material

The choice of load material for the simulation is ginger, which is a high value herbal crops (HVHC) in Malaysia (Othman et al.). Ginger is a popular and widely use medical herb in Malaysia which has many health benefits. However, ginger has a high moisture content which can create problems for storage and transportation, increasing the needs of developing a preservation technique (Depiver and Mallik, 2023). High moisture product can make the product susceptible to spoil and microbial growth such as fungi leading to the deterioration of the ginger. Moreover, ginger is stored in a bulk volume within a closed space that increases the spoilage rate due to the increase in moisture content. It is critical that the ginger's moisture content to be controlled at an acceptable level for storage and transportation. In the simulation, the ginger is designed to be cylinder-shaped with a radius of 0.04 m and a height of 0.02 m. There are 25 gingers for each tray shelves of the simulation. The ginger arrangement on the tray is shown in Figure 2.

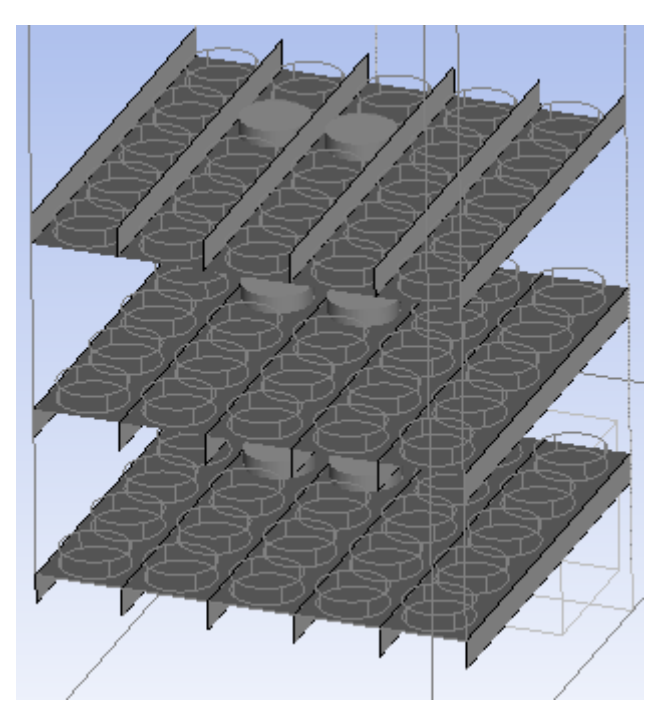


Figure 2. Ginger arrangement on the tray shelves inside the drying chamber.

# 2.3. Numerical Modelling

## 2.3.1. Governing Equation for CFD Model

The CFD model of heat transfer and airflow for the solar drying system is governed by the continuity equation, momentum equation and energy equation. These equations are able to numerically simulate the solar drying system performance under the boundary conditions given. The numerical equation for CFD is as follows.

# 2.3.2. Continuity Equation

In this modelling, the continuity can be expressed as an equation given below based on the principle of 'mass cannot be destroyed'. This particular equation holds significant value in the design and optimization of the solar drying chamber because of the utilization of air properties and volume of the system. It demonstrates that differences in density of air over time (t) are offset with differences in the airflow rates across the constraints of a control volume (solar drying chamber). Moreover, the equation is also crucial for fans which adopts airflow rate as a parameter to formulate velocity inside the solar drying chamber. In essence, the equation highlights the relationship between mass conservation such as

air properties and the volume of the material.

$$\frac{\partial \rho}{\partial t} + \frac{\partial (u)}{\partial x} + \frac{\partial (\rho v)}{\partial y} + \frac{\partial (\rho w)}{\partial z} = 0$$

Now, assuming that the flow is incomprehensible, the continuity equation can be expressed as follows (Gyawali et al., 2022):

$$\frac{\partial u}{\partial x} + \frac{\partial v}{\partial y} + \frac{\partial w}{\partial z} = 0 \tag{1}$$

where: ρ is density (kg m<sup>-3</sup>), u, v and w are velocities in the x, y, z directions, respectively.

# 2.3.3. Momentum Equation

In this simulation, the momentum equation plays a crucial role in analysing the motion of air with the atmospheric dynamics. It takes into consideration several factors such as pressure, gravity and viscosity to determine the acceleration experienced by the air. Hence, the momentum of air experiences fluctuations due to the combined influence of these forces. The equation represents both inertial forces (left-hand side equation) and viscous forces (right-hand side equation) for showcasing the motion of air respond to the internal and external forces. The equation allows predictions air behaviour in varying conditions. It proves to be useful where fan being used as a component in the system acting as a force in varying condition. Furthermore, it also provides an understanding towards the airflow patterns changes when operating for designers to be able to optimize and achieve the desired performance. x-momentum equation

$$\rho \left( u \frac{\partial u}{\partial x} + v \frac{\partial u}{\partial y} + w \frac{\partial u}{\partial z} \right) = \frac{\partial p}{\partial x} + \frac{\partial}{\partial x_i} \left[ (\mu + \mu_T) \left( \frac{\partial u}{\partial x_i} + \frac{\partial u_j}{\partial x} \right) \right]$$
(2)

y-momentum equation

$$\rho \left( u \frac{\partial v}{\partial x} + v \frac{\partial v}{\partial y} + w \frac{\partial v}{\partial z} \right) = \frac{\partial p}{\partial y} + \frac{\partial}{\partial x_i} \left[ (\mu + \mu_T) \left( \frac{\partial u}{\partial x_i} + \frac{\partial u_j}{\partial y} \right) \right]$$
(3)

z-momentum equation (Selimefendigil et al., 2023)

$$\rho \left( u \frac{\partial w}{\partial x} + v \frac{\partial w}{\partial y} + w \frac{\partial w}{\partial z} \right) = \frac{\partial p}{\partial z} + \frac{\partial}{\partial x_j} \left[ (\mu + \mu_T) \left( \frac{\partial u}{\partial x_j} + \frac{\partial u_j}{\partial z} \right) \right] \tag{4}$$

# 2.3.4. K-epsilon $(k - \varepsilon)$ Equation

In the  $k - \varepsilon$  model, two equations are incorporated into the design and simulation of the system. The turbulence kinetic energy (k) equation and the rate at which velocity fluctuations dissipate equation  $(\varepsilon)$ . (Gbegudu et al., 2022) The equations are crucial for assessing turbulent flows of a system such as pressure drops and velocity profiles. The equations are adopted where turbulence plays a role in the design and optimization of the system to improve efficiency and performance. It helps with anticipating the airflow against the PVTET system heatsink for heat retention and the ginger (porous media).

$$\frac{\partial}{\partial t}(\rho k) + \rho(\vec{v} \cdot \nabla)k = \nabla \cdot \left[ \left( \mu + \frac{\mu_t}{\sigma_k} \right) \nabla k \right] + P_k - \rho \varepsilon \tag{5}$$

$$\frac{\partial}{\partial t}(\rho\varepsilon) + \rho(\vec{v}\cdot\nabla)\varepsilon = \nabla\cdot\left[\left(\mu + \frac{\mu_t}{\sigma_\varepsilon}\right)\nabla\varepsilon\right] + C_{1\varepsilon}\frac{\varepsilon}{k}P_k - C_{2\varepsilon}\rho\frac{\varepsilon^2}{k}$$
(6)

#### 2.3.5. Energy Equation

$$\frac{\partial(\rho E)}{\partial t} + \nabla \cdot \left(\vec{u}(\rho E + P)\right) = \nabla \cdot \left(-\vec{q} + \bar{\bar{t}} \cdot \vec{u}\right) + S_h \tag{7}$$

The total energy of a system is the sum of its internal energy, which is the energy associated with the random motion of its particles, and its kinetic energy, which is the energy of motion of the system as a whole and can be expressed as follows:(Getahun et al., 2021).

$$E = h - \frac{P}{\rho} + \frac{u^2}{2}$$

where: E is total energy, h is sensible enthalpy of air (J/kg), q is heat flux (W m-2) and  $S_h$  is heat source terms (W/m³)

## 2.3.6. Porous media modelling

In the simulation, the process of drying the ginger in solar drying system involves complex interactions. The ginger in the simulation is considered to be a porous media in the solar drying system(Wang et al., 2021). This is because the momentum equation for the fluid flow through the ginger (porous media) needs to consider and can be expressed as a power-law method for calculating the pressure drop across the porous media:(Chaiworapuek et al., 2021)

$$\Delta p = C v^n \tag{8}$$

where: C and n are constant,  $\Delta p$  is pressure drop across porous (Pa) and v is velocity (m s<sup>-1</sup>)

# 2.3.7. Species Transport Modelling

In the simulation, the drying process especially the moisture removal transfer from the ginger to the surrounding environment is modelled through species transport equation. The species transport equation is to predict the mass fraction of H2O in the flow field through a convection-diffusion equation for the H2O mass fraction. The equation allows the simulation of the quantify the movement of moisture in the solar drying system and to predict the effectiveness of the solar drying system in removing the moisture from the ginger. The equation can be expressed as follows: (Daş et al., 2021)

$$\frac{\partial}{\partial t} \left( \rho Y_{H_2O} \right) + \nabla \cdot \left( \rho \vec{v} Y_{H_2O} \right) = -\nabla \cdot \overrightarrow{J_{H_2O}} + R_{H_2O} + S_{H_2O} \tag{8}$$

where: RH<sub>2</sub>O is H<sub>2</sub>O net rate of production, SH<sub>2</sub>O is H<sub>2</sub>O net rate of creation by addition of dispersed phase and any user-defined sources and  $\vec{v}$  is the velocity of the diffusing species (m s<sup>-1</sup>).

In the simulation, the drying load (porous media) from eq. 8 in the system represent the mass of water vapor in ginger and given an intended initial source term (moisture content) determined by trial-and-error simulation to ensure the value is similar to ginger's relative humidity of around 80%. RH2O represents the creation or destruction of water vapor (H<sub>2</sub>O) due to thermodynamic properties such as pressure, temperature and chemical composition within the system. Hence, RH<sub>2</sub>O plays a huge role in depleting or adding the moisture to the ginger until it reaches a thermodynamic equilibrium. Meanwhile, SH<sub>2</sub>O represents the external sources of water vapor independently formed such as 100% inlet relative humidity. 100% inlet relative humidity was intended in the simulation to produce a continuous H<sub>2</sub>O to ensure the overall humidity in the drying chamber over time.

#### 2.3.8. Numerical Solver

The model of the solar drying system with TEHP is created in ANSYS® Spaceclaim<sup>TM</sup> and to simulate the thermal analysis under different fan locations by using ANSYS® Fluent<sup>TM</sup>. The model selected for the program is the energy equation and k-epsilon viscous model equation. The simulation was initialized using the SIMPLE solution method. After calculation of the simulation, the temperature, velocity, heat flux, mass, momentum and  $H_2O$  mass fraction are obtained. Temperature and airflow contours of the solar drying system with TEHP were obtained. Solar drying systems with different fan locations and fan speeds are analysed under steady-state condition. Then, the best fan location with different fan speed is analysed under transient condition for understanding the effect of humidity over time.

# 2.3.9. Boundary Conditions

Several boundary conditions and assumptions are being used for the modelling of the solar drying

system with TEHP. The TEHP is based on A-200-24-44 manufactured by Laird Thermal System. The Th of the TEHP and the heatsink of the PVTET system are placed within the airflow channel for air to absorb heat and transfer it to the drying chamber of the solar dryer. The Th is set at 50 °C, simulating the desired heating temperature during operation, while the Tc is currently ignored. The initial moisture content is set at 0.1571 g/s, calculated from the ginger's relative humidity of around 80%. The panel temperature of the PVTET system is set at 60 °C. In the ANSYS® Fluent<sup>TM</sup> software, the airflow for the fan is varied from 0.003, 0.006, 0.009, up to 0.012 m³/s, to study the effect of airflow on the temperature and H2O mass fraction of the drying product and chamber, ultimately determining the drying rate. The flow inlet is set with a relative humidity of 100%, where the temperature and H2O mass fraction at the outlet and on the drying product are then obtained for discussion.

## 2.4. Validation of the Numerical Model

In order to validate the CFD simulation mode, the results obtained from the simulation of the drying process of ginger are analysed in relation to existing drying models from previous studies of (Ndukwu et al., 2023) and (Suherman et al., 2021). Two specific drying models have been considered for comparative study, primarily because their experimental conditions closely align with the boundary conditions established in our simulation. This is crucial as it allows for a more accurate evaluation and understanding of the drying behaviour of ginger under similar parameters, thereby enhancing the validity of the comparison and provide deeper insights into the effectiveness of the simulation models in question.

### 3. Results and Discussion

A thorough examination of the results obtained from the analysis is conducted with the primary objective to critically evaluate the quality of the validation process. The sections serve as detailed accounts of the research findings, providing insights into the validity of the conclusions drawn from the study. Subsequent analysis throughout the discussion will focus on the optimized design discussed in the previous section. In the discussion, the location of measurement for temperature and relative humidity is essential for accurate analysis and comparison of the drying operation. The simulated drying system has 25 multiple points located in each of the upper, middle, and bottom shelves of the chamber for every drying product to monitor the temperature and relative humidity gradients. The results generated from multiple points are averaged to represent the overall conditions of the results gained. The average measurement enables us to grasp a more thorough insight into the mechanism of the drying environment condition within the solar dryer.

#### 3.1. Mesh Independence Study

Mesh independence study has been generated for the solar drying system as illustrated by Figure 3 to ensure an accurate model of the system. A hexahedral mesh of the studied model has been generated. The mesh refinement generated by ensuring the X, Y and Z grid size for 2.4 million element such as 0.01875, 0.04425 and 0.04268 are times with 1.5 to refine the mesh. The air outlet temperature was generated for every grid as shown in Figure 3. The mesh study focused on the solar drying system with a fixed boundary conditions to ensure a precise comparison of the grid. According to the Figure 3 the temperature is consistent at ~48.4 °C at 2.5 million element and then the temperature fluctuates as the grid increased. Thus, the mesh with 2.5 million element was used in the simulation for every case. Table 3 showcase the mesh parameters use for the grid independence test.

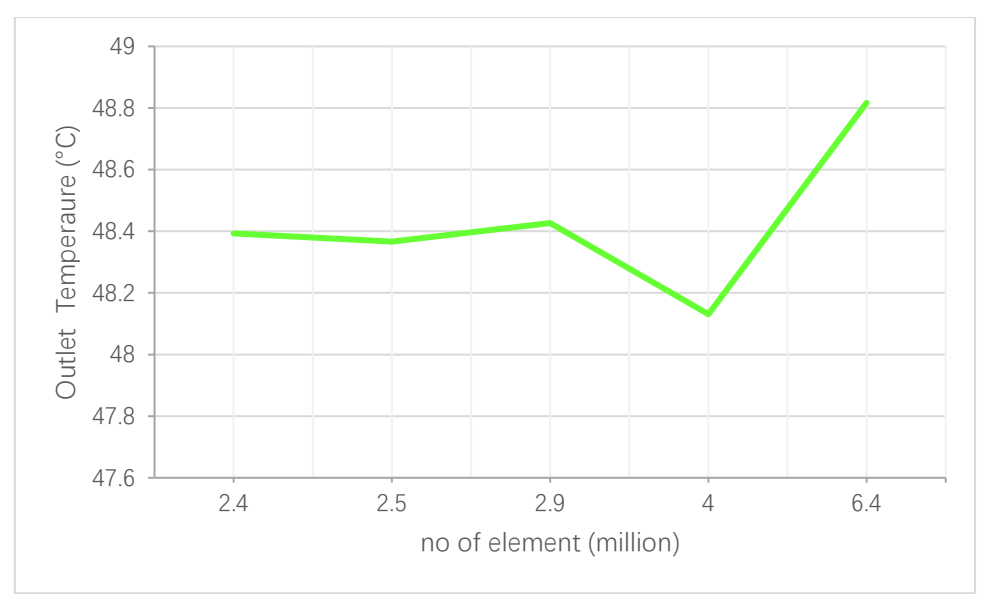


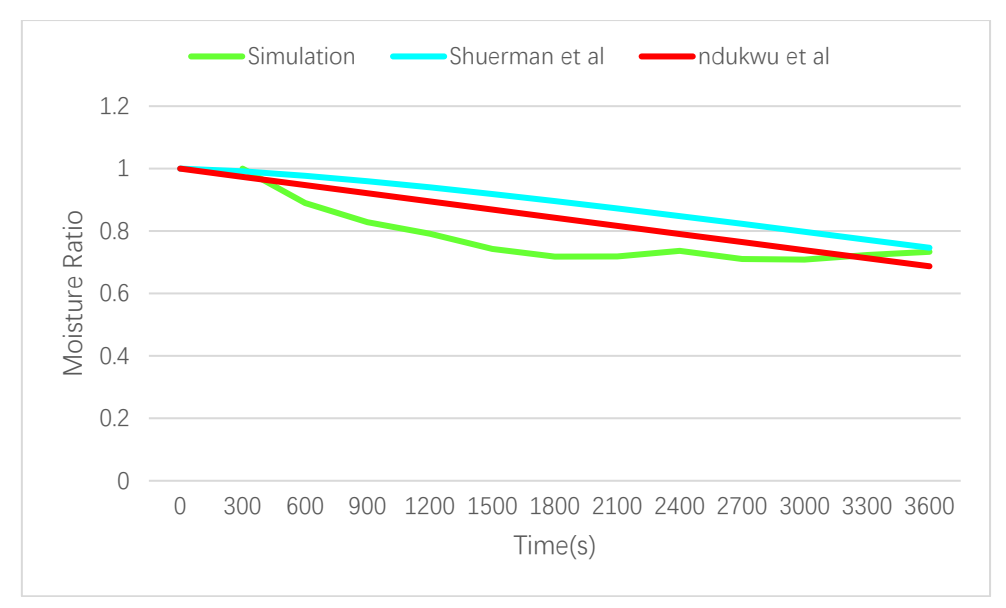
Figure 3. Mesh Independence Study results.

Table 3. Mesh Parameters.

Flow rate	X Grid Size	Y Grid Size	Z Grid Size	No of element (million)
0.00300	0.01875	0.04425	0.04268	2.4
0.00300	0.01250	0.02950	0.02845	2.5
0.00300	0.00833	0.01967	0.01897	2.9
0.00300	0.00556	0.01311	0.01264	4.0
0.00300	0.00370	0.00874	0.00843	6.4

# 3.2. Validation of the Numerical Model

To validate our CFD model, the boundary conditions were set at a drying temperature of 60 °C and an initial ginger moisture content of 80%, consistent with the study by Ndukwu et al. (2023). In their research, they experimented with a hybrid solar dryer equipped with thermal storage for ginger drying. They developed a moisture ratio equation to represent the experimental data for unblanched ginger drying. This equation, a logarithmic model with an R² value of 0.9875, was calculated and compared with our simulation results. Ndukwu et al. identified this as the best model for unblanched ginger. Similarly, Suherman et al. (2021) investigated a hybrid solar dryer for ginger drying, analyzing the drying process at various temperatures to assess dryer performance and dried ginger quality. They derived moisture ratio equations for temperatures of 40, 50, and 60 °C. The equation for 60 °C, a Page model with an R² value of 0.995, was used for comparison with our results. This model was deemed the most accurate for predicting ginger drying behavior at 60 °C. The moisture ratios from our simulation and other models, along with their relative errors, are presented in Table 4. Figure 4 illustrates the moisture ratio values over time for both the simulation and the drying models. The alignment between our simulation results and these established models demonstrates the credibility of our CFD model for practical applications in ginger drying processes.



*Figure 4.* Comparison of moisture ratio with time by simulation with other drying models (Ndukwu et al., 2023) and (Suherman et al., 2021).

Table 4. Relative error of moisture ratio.

Time(s)	MR from simulation	MR from (Suherman et al., 2021).	MR from (Ndukwu et al., 2023)	Relative error (Suherman et al., 2021) [%]	Relative error (Ndukwu et al., 2023) [%]
0	-	1	1	-	-
300	1	0.974	0.991	2.64	0.87
600	0.890	0.947	0.977	6.45	9.79
900	0.828	0.921	0.960	11.20	15.86
1200	0.791	0.895	0.940	13.05	18.76
1500	0.743	0.869	0.919	16.98	23.71
1800	0.718	0.842	0.896	17.33	24.77
2100	0.719	0.816	0.872	13.63	21.41
2400	0.736	0.790	0.848	7.36	15.17
2700	0.710	0.765	0.823	7.61	15.84
3000	0.708	0.739	0.798	4.26	12.59
3300	0.723	0.713	0.772	1.41	6.79
3600	0.734	0.687	0.746	6.34	1.75

# 3.3. Impact of fan Location on the TEHP Assisted Solar Drying System

In this section, the findings in this study provide insights related to the different fan location in the solar drying system implications and its particular relevant. The outcomes derived from the solar drying system simulation with different fan locations with different fan speeds are showcased in graphs within their designated sections.

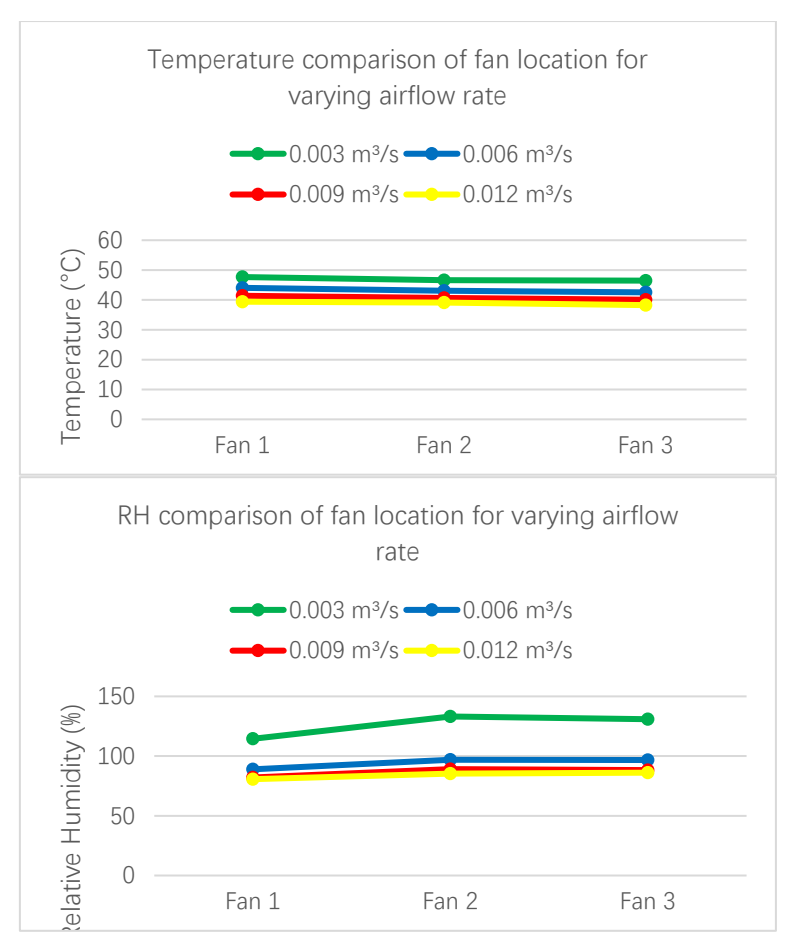


Figure 5. Temperature (a) and Relative Humidity (b) of the outlet at different fan locations for the solar drying system.

Based on the results obtained (Figure 5), different fan locations do have a significant impact on the temperature and relative humidity of the solar drying system. According to Figure 5a, Fan 1 seems to have the highest temperature as to compare to Fan 2 and Fan 3 at varying airflow rates. The temperature outlet for Fan 1 is 48 °C at an airflow rate of 0.003 m3/s, in contrast to the temperatures for Fan 2 and Fan 3, which is around 46 °C. Furthermore, this pattern persists as the flow velocity continues to escalate. This is because Fan 1 location at the system inlet enables it to gather the convective heat more evenly from the PVTET before flowing into the drying chamber. In addition, Fan 1's relative humidity (%RH) is the lowest compared to Fan 2 and Fan 3 (Figure 5b). This is because Fan 1 allows a better airflow distribution for humidity to move from the drying chamber towards the outlet. This reduced %RH ensures more efficient moisture removal from the drying product and flows out of the drying chamber as compared to Fan 2 and Fan 3, where their relative humidity is high. Based on the result obtained, the optimal fan location is identified as Fan 1, which creates the best thermal environment for the drying chamber with the best reduction in relative humidity.

# 3.4. Impact of Different Airflow Rate in the TEHP Assisted Solar Drying System on Moisture Removal

Figure 6 shows the decreasing H<sub>2</sub>O mass fraction in the drying process during transient simulations for each tray shelves. The biggest reduction happened on the bottom tray shelf since it is the first to interact with the hot air coming from the TEHP. In Figure 6a, the H<sub>2</sub>O mass fraction of the lower shelf when the airflow rate is 0.003 m<sup>3</sup>/s is higher than when the airflow rate is 0.012 m<sup>3</sup>/s. This is because the lower airflow rate is able to let the moisture from the ginger stays longer inside the chamber before travelling into the outlet. The middle and upper tray shelves have almost similar reduction, except at 0.003 m<sup>3</sup>/s. This is because the H<sub>2</sub>O mass from the lower shelf risen upwards, affecting the middle and upper shelves. Moreover, it can also be observed that the higher the airflow rate, the higher the amount of moisture being removed due to increased convective heat transfer between the air and the ginger. Based on the result obtained, the optimal airflow rate is identified as 0.012 m<sup>3</sup>/s, which creates the best

drying rate for the chamber with the lowest H<sub>2</sub>O mass fraction.

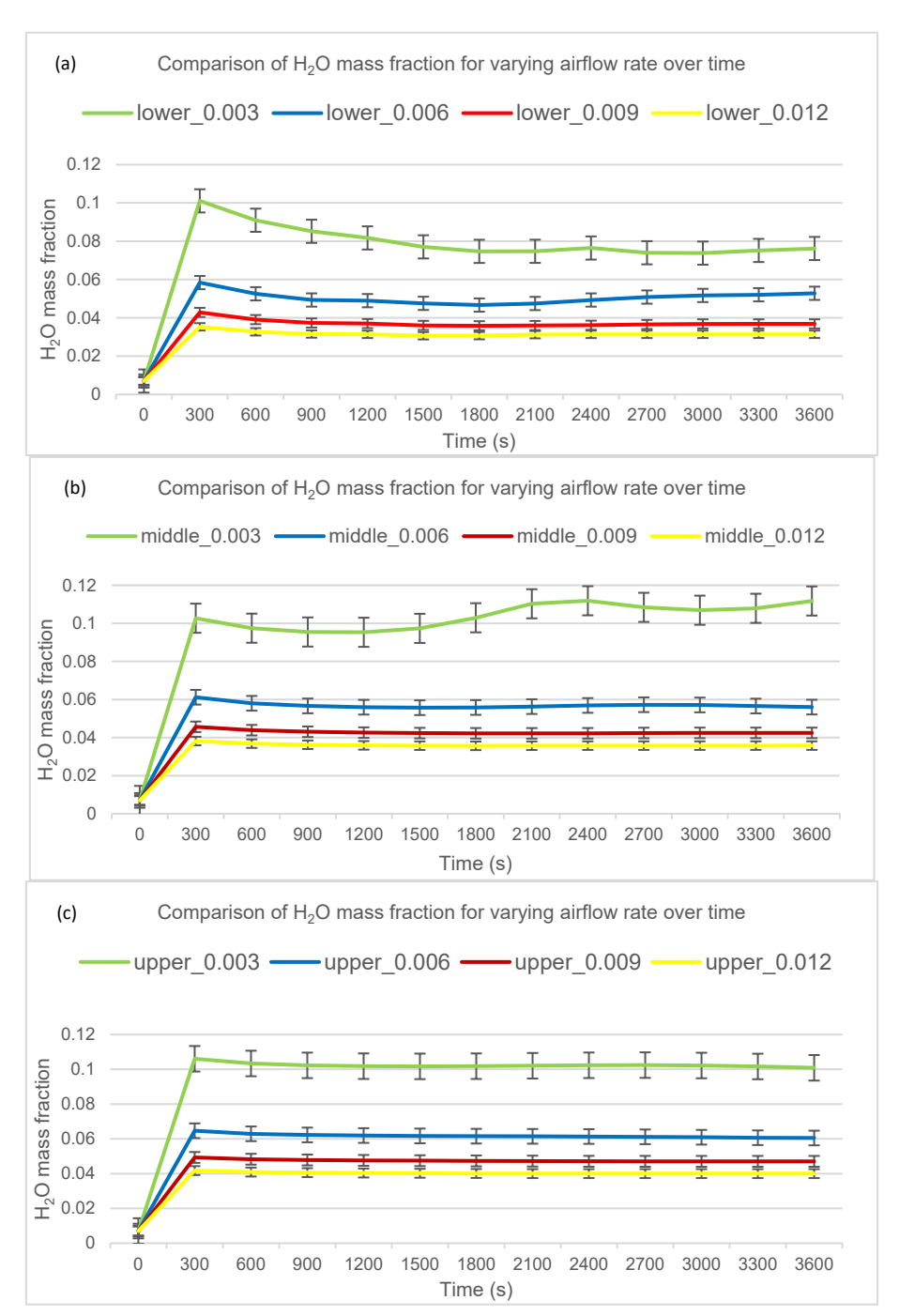


**Figure 6.**  $H_2$  O mass fraction of ginger for TEHP assisted solar drying system at different airflow rates at the bottom tray shelf (a), middle tray shelf (b) and upper tray shelf (c).

# 3.5. Impact of Different Airflow Rates on Temperature Distribution in the TEHP Assisted Solar Drying System

Figure 7 shows the increase of the ginger's temperature in the drying process during transient simulations for each tray shelves. The temperature observed on the bottom tray shelf ( $\sim$ 46 °C) is the highest since the bottom shelf is the first to interact with the hot air coming from the solar drying system. In Figure 7a, the temperature of the lower shelf when the airflow rate is 0.003 m³/s is higher than the lower shelf when the airflow rate is 0.012 m³/s. This is because the flow able to let the temperature carried from the PVTET system and TEHP stay longer inside the chamber before flowing to the outlet. The middle and upper trays have similar temperatures, except when the airflow rate is 0.003 m³/s, especially in the middle tray (Figure 7b). This might be due to the low airflow rate, resulting in uneven temperature

distribution between the drying products. However, as the airflow rate increases, air distribution becomes more stable. Results suggest that for an even air distribution of the drying products, heat transfer should be controlled from the lower tray shelf and air from the PVTET system and TEHP should be directed more towards the middle and upper tray shelf, else there would be asymmetrical drying performance throughout the chamber.

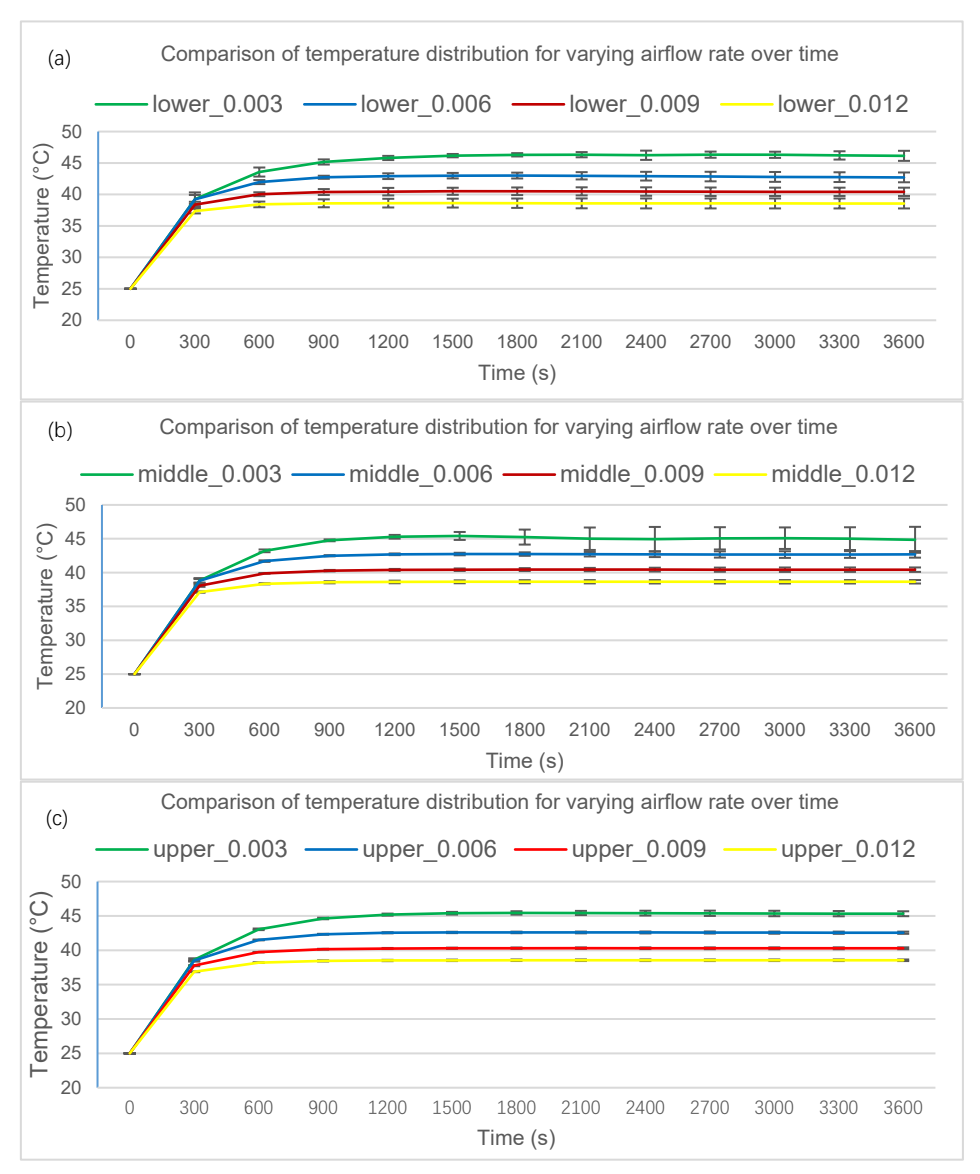


Figure 7.  $H_2O$  mass fraction of ginger for TEHP assisted solar drying system at different airflow rates at the bottom tray (a), middle tray (b) and upper tray (c).

# 3.6 Temperature Distribution of Ginger Slices

Figure 8 shows the ginger's temperature distribution in the drying process for fan 1 with 0.003 m3/s during transient simulations for each tray shelves. It is evident that the temperature of the ginger exhibited variation based on the placement on the trays within the drying chamber, showcasing the impact of positioning on the temperature distribution of the drying chamber. The temperature gradients were distinct across the different trays of the drying chamber, underscoring the non-uniform distribution of heat throughout the system. Moreover, the temperature distribution among the drying products produced a distinct pattern. The majority of the drying products on the tray below exhibited high temperatures and the middle and upper tray exhibited lower temperatures. According to Figure 8, the drying product after 10 minutes shows around 44–45 °C but three rows of the drying product at the below tray shows around 45–47 °C due to its placement being very near to the TEHP. After 20 minutes, the temperature distribution becomes more uniform and the drying product at the below tray exhibited temperature around 46–48 °C, and the middle and upper trays started to increase their temperature around 46 °C. It is to be

noted that the heat travels towards the middle due to the fan pushing the heat to the other row. After 30 minutes, the temperature distribution increases around 47–48 °C for the tray below and 46–47 °C for the middle and upper trays. However, the temperature distribution slowly decreases for the tray below after 40 minutes, since moisture has been evaporated from the tray and moving towards the middle and upper tray before being removed from the system. After 40 minutes, the temperature for the middle and upper trays increased around 47 °C, the same as the tray below. After 50–60 minutes, the temperature decreases more uniformly for the middle and upper trays, but is non-uniformly distributed at the tray below, due to the placement near to the fan where they are colder. Based on the result obtained, the drying load has an inhomogeneous temperature distribution as the air channel went through the three tray shelves. This led to uneven drying to the product on each shelf and not sustainable for the drying system. Therefore, further studies should focus on structural parameters such as the number of loads and shelves, drying chamber dimensions, and drying system configurations.

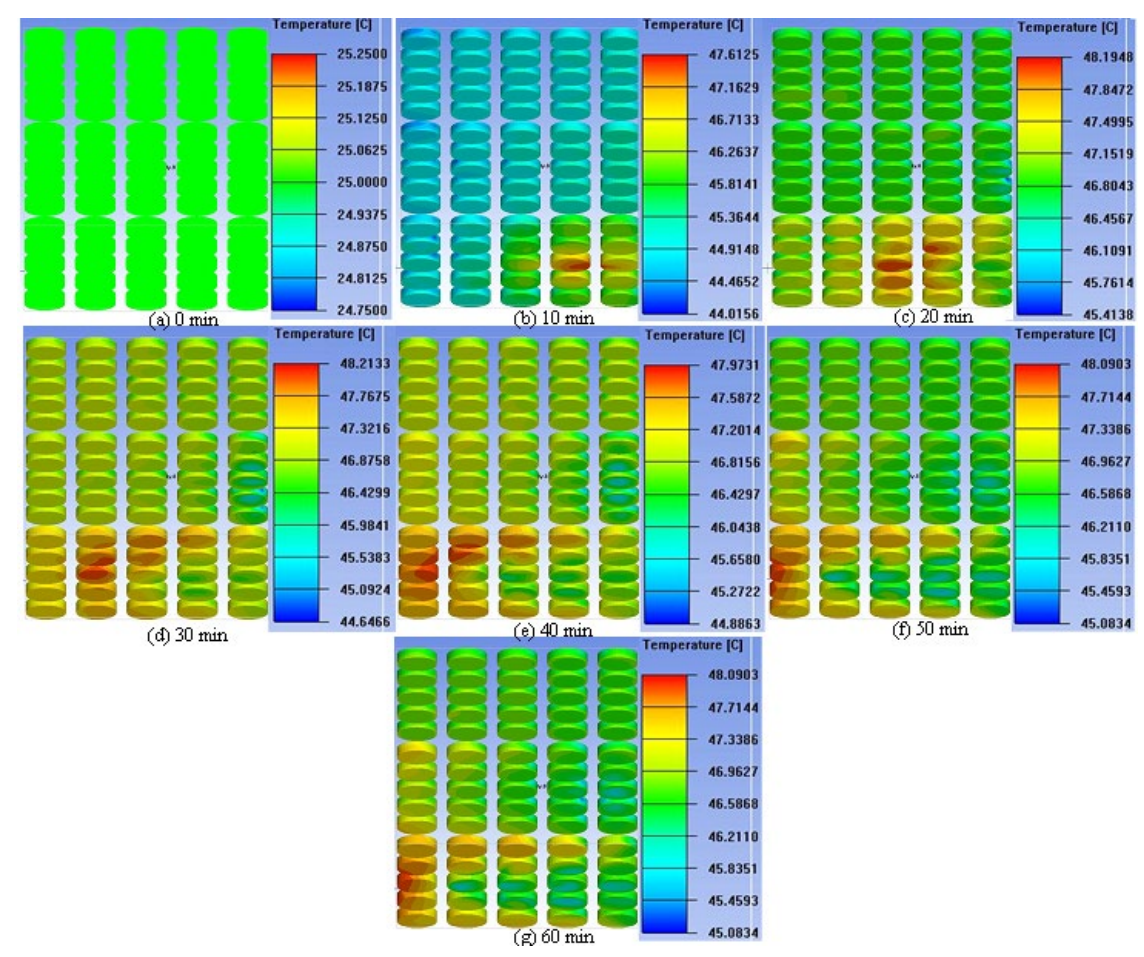


Figure 8. Temperature profile of ginger slices during drying in TEHP-assisted solar drying system (a) 0 min (b) 10 min (c) 20 min (d) 30 min (e) 40 min (f) 50 min (g) 60 min.

# 3.7. Velocity Distribution of Drying Chamber and Tray

Figure 9 shows the velocity distribution of drying chamber and tray in the drying process for fan 1 with 0.003 m³/s during transient simulations. It is evident that the velocity of the drying chamber and tray exhibited variation within the drying chamber and tray, showcasing the impact of airflow rate to the drying rate of the drying chamber. The circulating airflow were distinct across the different trays of the drying chamber. Most of the circulating airflow moves along the bottom tray and the sidewall of the drying chamber before being drawn to the outlet at the top of the drying chamber. Moreover, the circulating airflow produced a distinct pattern, the volume of circulating air flows from the bottom tray and directly towards the outlet from the sidewall without flowing through the middle and top tray drying chamber. This exhibits a low circulating air reducing the drying rate for the middle and top tray drying chamber.

According to Figure 9, the drying chamber and tray after 10 minutes shows around 0 - 0.125 m/s for the top and middle tray, but the below tray shows around 0-1 m/s due to the bottom tray being very near

to the TEHP. However, the circulating airflow is unable to fully circulate the bottom tray and the sidewall. After 20 minutes, the circulating airflow becomes more uniform at the bottom tray and at the sidewall of the drying chamber and exhibited a velocity around 0.25–1 m/s. The middle and upper trays started to increase their velocity around 0.25 m/s. However, the airflow does not circulate around the middle and upper tray and instead move towards the outlet from the sidewall. After 30 minutes, the circulate air become more uniform for the bottom tray with the sidewall. In addition, the velocity of the middle tray increases around 0–0.25 m/s but the air only circulates near the sidewall.

For the upper tray, the circulate air flows at the sidewall of the drying chamber towards the outlet. After 40 minutes, the bottom tray exhibits the same circulation as before, but the circulating air slowly circulate uniformly for the middle tray. The top tray still exhibits a low air circulation with the air only moving at the sidewall near the outlet. After 60 minutes, the velocity increase at the sidewall near the bottom tray at around 0.5–1 m/s. However, the bottom and top tray only exhibits a velocity around 0–0.25 m/s. Based on the result obtained, it is evident that the drying chamber has an inhomogeneous velocity distribution as the air went through the three trays, leading to uneven drying to the product on each shelf.

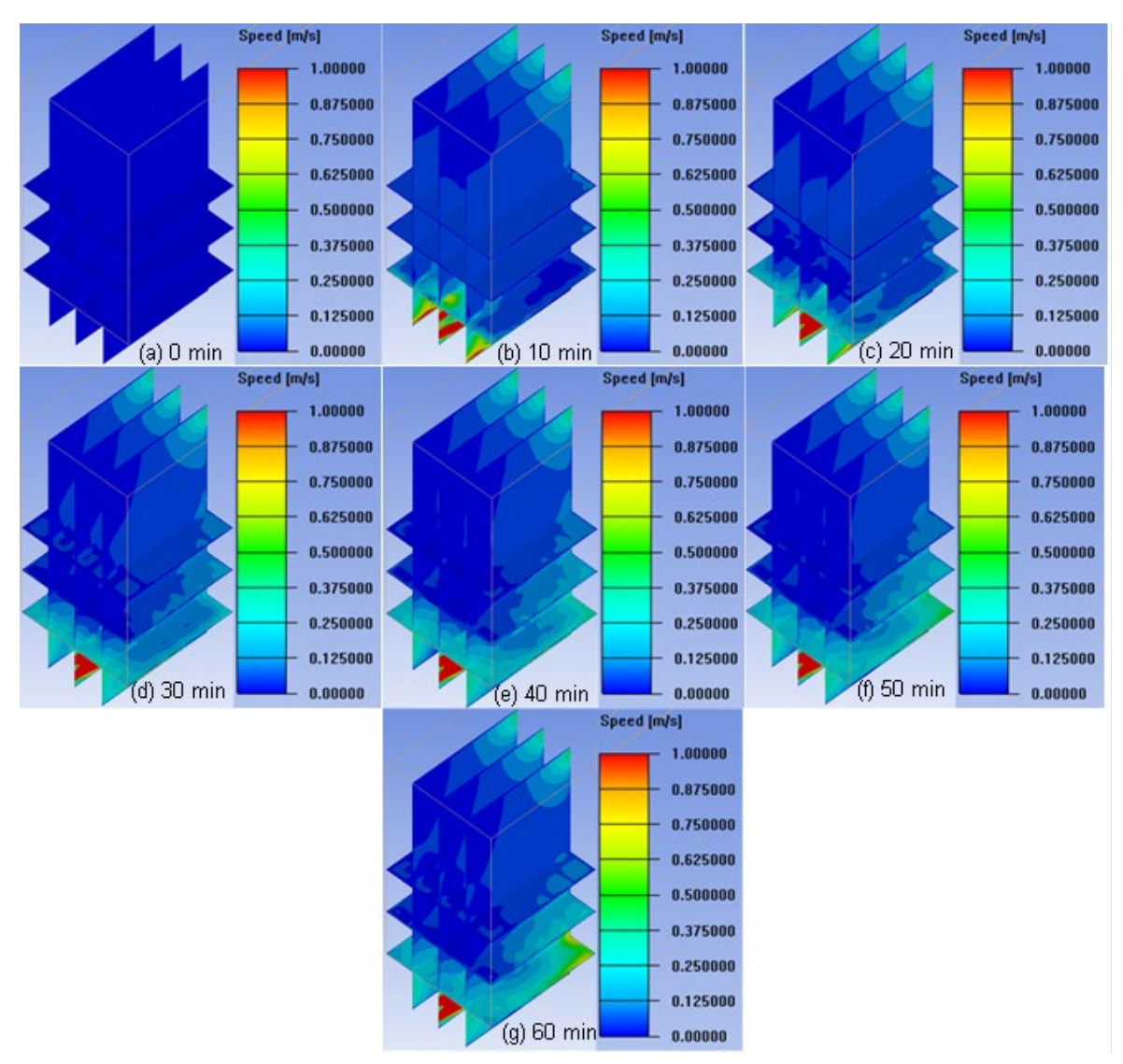


Figure 9. Contours of velocity distribution on the dryer chamber and tray during drying at (a) 0 min (b) 10 min (c) 20 min (d) 30 min (e) 40 min (f) 50 min (g) 60 min.

# 3.8 Temperature Distribution of Drying Chamber and Tray

Figure 10 shows the temperature distribution on the drying chamber and tray drying process for fan 1 with 0.003 m<sup>3</sup>/s during transient simulations. It is evident that the temperature of the drying chamber and tray exhibited variation, showcasing the impact of position on the temperature distribution of the

drying chamber. The temperature gradients were distinct across the different trays of the drying chamber, underscoring the non-uniform distribution of heat throughout the system. Moreover, the temperature distribution among the tray produced a distinct pattern. The tray below exhibited high temperatures, and the middle and upper tray exhibited lower temperatures. According to Figure 8, the solar dryer and tray after 10 minutes shows around 41–45 °C but the bottom tray shows around 43–45 °C due to its placement being very near to the TEHP. After 20 minutes, the temperature distribution increases for the solar dryer and becomes more uniform at around 45–47 °C and the bottom tray exhibited temperature around 46–47 °C, and the middle and upper trays started to increase their temperature around 46 °C.

After 30 minutes, the temperature distribution increases around 47–48 °C for the drying chamber and tray. However, the bottom tray exhibited the highest temperature compared to the middle and upper tray of the drying chamber. After 40 minutes, the temperature distribution for the middle and upper trays increased around 47 °C, the same as the tray below. However, the left side contour of the drying chamber exhibits a temperature around 45 °C compared to the middle and right contour of the drying chamber. This illustrated that the temperature only circulates around the middle and right contour of the drying chamber. Past 50 minutes mark shows the same temperature distribution as the 40 minutes mark. Based on the result obtained, the drying chamber has an inhomogeneous temperature distribution as the air channel went through the three tray shelves, also leading to uneven drying to the product on each shelf. Moreover, the results obtained from the simulation shows the importance of identifying inadequate temperature regions of the drying chamber and tray.

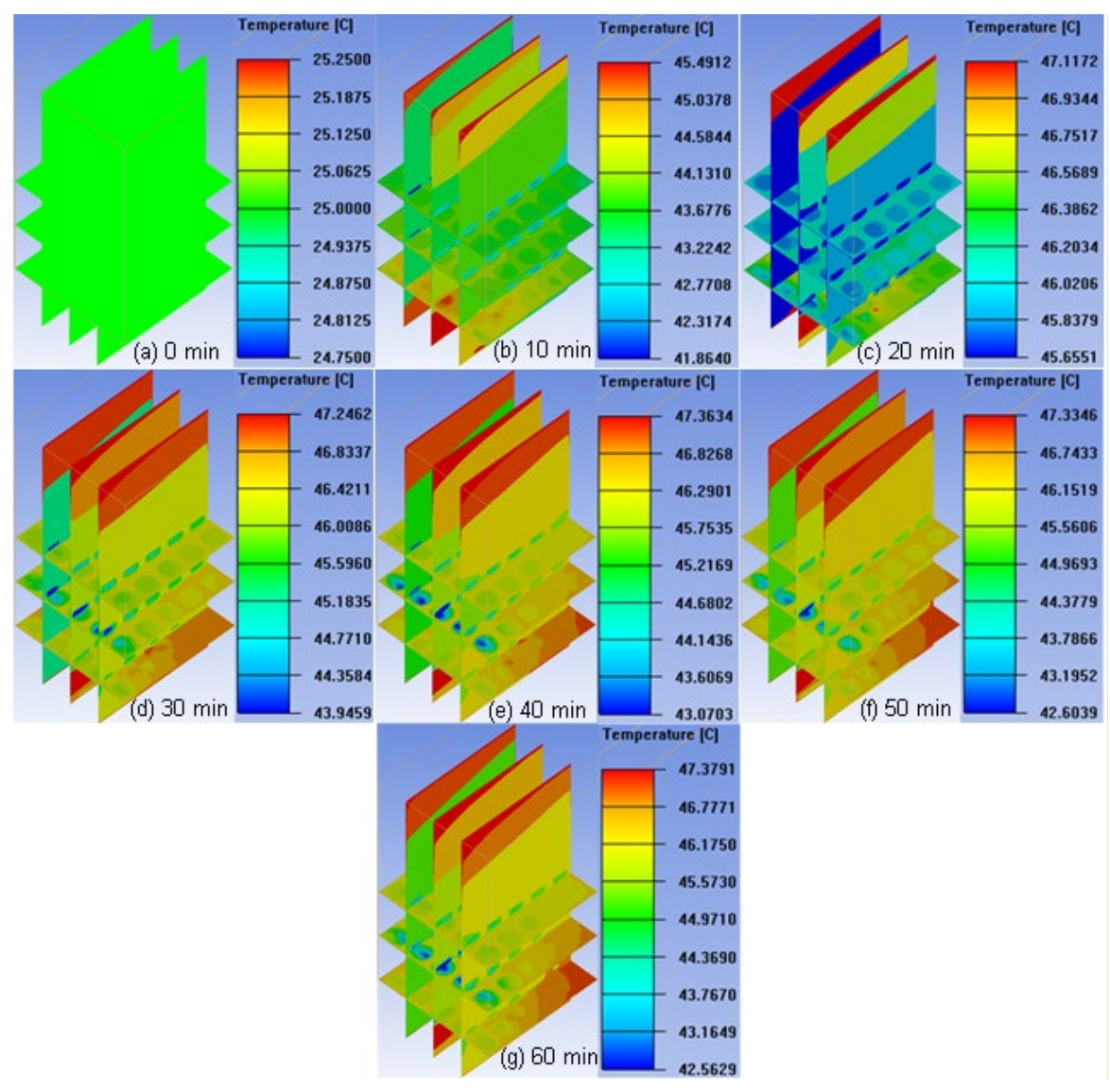


Figure 10. Contours of temperature distribution on the drying chamber and tray during drying at (a) 0 min (b) 10 min (c) 20 min (d) 30 min (e) 40 min (f) 50 min (g) 60 min.

### 4. Conclusion

In this study, the impact of the fan location and airflow rate on the drying rate of TEHP assisted solar drying systems are investigated. The CFD simulation is proven to reduce the development time and ensure performance by considering the dynamic characteristics of the solar drying system. The temperature, relative humidity and  $H_2O$  mass fraction in working conditions have been predicted and discussed, finding the optimum condition for the solar drying system configuration. The following conclusion was drawn from the study:

- 1) TEHP-assisted solar drying system with Fan 1 location shows the best temperature distribution and faster drying rates.
- 2) Greater airflow rate reduces the relative humidity, H<sub>2</sub>O mass fraction and accumulated heat inside the chamber, resulting in faster drying rates.
- 3) Airflow rate of 0.012 m<sup>3</sup>/s showed the lowest H<sub>2</sub>O mass fraction, resulting in faster drying rates.
- 4) The drying process in a vertically drying chamber is heavily influenced by airflow and product arrangement. Drying rates across shelves are inconsistent due to the uneven distribution of temperature and flow affecting the product quality. Thus, the ideal product configuration is crucial for optimal drying rate.

Based on the conclusion presented, the airflow rate needs to be carefully optimized in any given system design to ensure optimal drying rates, depending on the load given to dry, especially the intricate relationships of temperature and water content within the system. The findings of the study can be effectively utilized for strategic modification and refinements to enhance the overall system efficiency of a solar drying system, while reducing potential thermal losses and offering a sustainable solution by integrating with TEHP and PVTET systems to advance the solar drying technology. Therefore, future studies should focus on structural parameters such as duct configuration, damper-based controls and localised fan clusters. Moreover, thermal performance such as integrating a thermal energy storage, waste heat recovery system and glazing selection. Future experimental work in assessing and proving the determined parameters of the solar dryer as the optimal parameters will be conducted.

**Funding:** The author would like to extend our gratitude towards Universiti Kebangsaan Malaysia for supporting this work under the grant GUP-2023-044. Additionally, this work has been accepted and presented at ISCREE 2024.

Conflicts of Interest: The authors declare no conflict of interest.

#### References

- Amjad, W., Munir, A., Akram, F., Parmar, A., Precoppe, M., Asghar, F., & Mahmood, F. (2023). Decentralized solar-powered cooling systems for fresh fruit and vegetables to reduce post-harvest losses in developing regions: a review. *Clean Energy*, 7(3), 635-653. https://doi.org/10.1093/ce/zkad015
- Chaiworapuek, W., Chuenboonma, N., Thungthong, T., Munprom, R., Sae-tan, S., & Onwimol, D. (2021). Numerical investigation of air flow in a vertically paddy bed dryer using computational fluid dynamics. *IOP Conference Series: Materials Science and Engineering*, 1137(1). https://doi.org/10.1088/1757-899x/1137/1/012066
- Cheon, S.-Y., Lim, H., & Jeong, J.-W. (2019). Applicability of thermoelectric heat pump in a dedicated outdoor air system. *Energy*, 173, 244-262. https://doi.org/10.1016/j.energy.2019.02.012
- D. Pagukuman, B. N., & Wan Ibrahim, M. K. (2021). A review of the significance effect of external factors of the solar dyer design to dried foods product quality. *Journal of Engineering, Design and Technology*, 20(6), 1765-1786. https://doi.org/10.1108/jedt-01-2021-0033
- Daş, M., Alıç, E., & Kavak Akpinar, E. (2021). Numerical and experimental analysis of heat and mass transfer in the drying process of the solar drying system. *Engineering Science and Technology, an International Journal*, 24(1), 236-246. https://doi.org/10.1016/j.jestch.2020.10.003
- Deng, Z., Li, M., Xing, T., Zhang, J., Wang, Y., & Zhang, Y. (2021). A literature research on the drying quality of agricultural products with using solar drying technologies. *Solar Energy*, 229, 69-83. https://doi.org/10.1016/j.solener.2021.07.041
- Depiver, J. A., & Mallik, S. (2023). An Empirical Study on Convective Drying of Ginger Rhizomes Leveraging Environmental Stress Chambers and Linear Heat Conduction Methodology. *Agriculture*, 13(7). https://doi.org/10.3390/agriculture13071322
- Diaz de Garayo, S., Martínez, A., Aranguren, P., & Astrain, D. (2021). Prototype of an air to air thermoelectric heat pump integrated with a double flux mechanical ventilation system for passive houses. *Applied Thermal Engineering*, 190. https://doi.org/10.1016/j.applthermaleng.2021.116801
- Ekka, J. P., Muthukumar, P., Bala, K., Kanaujiya, D. K., & Pakshirajan, K. (2021). Performance studies on mixed-mode forced convection solar cabinet dryer under different air mass flow rates for drying of cluster fig. Solar Energy, 229, 39-51. https://doi.org/10.1016/j.solener.2021.06.086
- Evstatieva, N. L., Belovski, I. R., & Aleksandrov, A. T. (2019). Optimization and Modelling of the Thermal Resistance of a Thermoelectric Pump Heat Sink. 10th National Conference with International

- Participation, ELECTRONICA 2019 Proceedings. https://doi.org/10.1109/ELECTRONICA.2019.8825590
- Fahruddin, A., Tjahjanti, P. H., & Mulyadi. (2022). Effect of Thermoelectric Power and Air Flow on Air Temperature and Relative Humidity. *Journal of Energy, Mechanical, Material, and Manufacturing Engineering*, 7(1), 21-26. https://doi.org/10.22219/jemmme.v7i1.21761
- Fernandes, L., & Tavares, P. B. (2024). A Review on Solar Drying Devices: Heat Transfer, Air Movement and Type of Chambers. *Solar*, 4(1), 15-42. https://doi.org/10.3390/solar4010002
- Gbegudu, J. K., Fetuga, I. A., Olakoyejo, O. T., Shitta, M. B., Siqueira, A. M. d. O., Akari, E. O., & Aderemi, K. S. (2022). Numerical simulation of forced convective fish drying performance of different cabinet geometry. 

  The Journal of Engineering and Exact Sciences, 8(6), 14666-14601i. 
  https://doi.org/10.18540/jcecvl8iss6pp14666-01i
- Getahun, E., Delele, M. A., Gabbiye, N., Fanta, S. W., Demissie, P., & Vanierschot, M. (2021). Importance of integrated CFD and product quality modeling of solar dryers for fruits and vegetables: A review. *Solar Energy*, 220, 88-110. https://doi.org/10.1016/j.solener.2021.03.049
- Gomez-Casanovas, N., Mwebaze, P., Khanna, M., Branham, B., Time, A., DeLucia, E. H., Bernacchi, C. J., Knapp, A. K., Hoque, M. J., Du, X., Blanc-Betes, E., Barron-Gafford, G. A., Peng, B., Guan, K., Macknick, J., Miao, R., & Miljkovic, N. (2023). Knowns, uncertainties, and challenges in agrivoltaics to sustainably intensify energy and food production. *Cell Reports Physical Science*, 4(8). https://doi.org/10.1016/j.xcrp.2023.101518
- Gyawali, M., Acharya, A., Adhikari, T., Dahal, K., Kafle, B., Kim, D. H., & Kafle, S. (2022). A mixed-mode ginger and turmeric solar dryer: design, simulation, biochemical and performance analysis. *BIBECHANA*, 19(1-2), 40-60. https://doi.org/10.3126/bibechana.v19i1-2.46386
- Herez, A. (2021). Systèmes hybrides photovoltaïque / thermique / thermoélectrique à concentrateur parabolique :modélisation thermique, analyse paramétrique et études de cas (Publication Number 2021ANGE0009) [PhD thesis, Université d'Angers]. Univ-angers Univ-angers-these Star Laris. https://theses.hal.science/tel-03412756
- Herrando, M., Wang, K., Huang, G., Otanicar, T., Mousa, O. B., Agathokleous, R. A., Ding, Y., Kalogirou, S., Ekins-Daukes, N., Taylor, R. A., & Markides, C. N. (2023). A review of solar hybrid photovoltaic-thermal (PV-T) collectors and systems. *Progress in Energy and Combustion Science*, 97. https://doi.org/10.1016/j.pecs.2023.101072
- Hii, C. L., Ong, S. P., Chiang, C. L., & Menon, A. S. (2019). A review of quality characteristics of solar dried food crop producst. *IOP Conference Series: Earth and Environmental Science*, 292(1). https://doi.org/10.1088/1755-1315/292/1/012054
- Hussain, A.-K., Tadahmun Ahmed, Y., & Sundus, A.-A. (2021). Thermal Analysis of Tilapia Fish Drying by Hybrid Solar Thermal Drying System. *Journal of Advanced Research in Fluid Mechanics and Thermal Sciences*, 90(1), 115-129. https://doi.org/10.37934/arfmts.90.1.115129
- Jaiswal, P., Anupam, B. R., Chandrappa, A. K., & Sahoo, U. C. (2023). Harvesting heat energy using geothermal and hydronic pavements for sustainable cities: A comprehensive review of an emerging idea. Sustainable Cities and Society, 93. https://doi.org/10.1016/j.scs.2023.104539
- Jalal Abduelgader, A., Ali, H. A. A., Hazem, M., Ag Sufiyan Abd, H., Ahnad, F., & Sopian, K. (2020). Solar Assisted Heat Pump System for High Quality Drying Applications: A Critical Review. *International Journal of Renewable Energy Research*, 10(1), 303-316. https://doi.org/10.20508/ijrer.v10i1.10403.g7876
- Kherrafi, M. A., Benseddik, A., Saim, R., Bouregueba, A., Badji, A., Nettari, C., & Hasrane, I. (2024). Advancements in solar drying technologies: Design variations, hybrid systems, storage materials and numerical analysis: A review. *Solar Energy*, 270. https://doi.org/10.1016/j.solener.2024.112383
- Lim, H., & Jeong, J. W. (2020). Numerical and experimental study on the performance of thermoelectric radiant panel for space heating. *Materials*, 13(3). https://doi.org/10.3390/ma13030550
- Martinez, A., Díaz de Garayo, S., Aranguren, P., & Astrain, D. (2019). Assessing the reliability of current simulation of thermoelectric heat pumps for nearly zero energy buildings: Expected deviations and general guidelines. *Energy Conversion and Management*, 198. https://doi.org/10.1016/j.enconman.2019.111834
- Mugi, V. R., & Chandramohan, V. P. (2021). Shrinkage, effective diffusion coefficient, surface transfer coefficients and their factors during solar drying of food products A review. *Solar Energy*, 229, 84-101. https://doi.org/10.1016/j.solener.2021.07.042
- Ndukwu, M. C., Augustine, E. B., Ugwu, E., Ibeh, M. I., Ekop, I., Akpan, G., Udo, A. E., Ihediwa, V. E., Akuwueke, L., Mbanasor, J., & Abam, F. (2023). Drying kinetics and thermo-economic analysis of drying hot water blanched ginger rhizomes in a hybrid composite solar dryer with heat exchanger. *Heliyon*, 9(2), e13606. https://doi.org/10.1016/j.heliyon.2023.e13606
- Othman, N. F., Mat Su, A. S., & Ya'Acob, M. E. (2018). Promising Potentials of Agrivoltaic Systems for the Development of Malaysia Green Economy. *IOP Conference Series: Earth and Environmental Science*, 146. https://doi.org/10.1088/1755-1315/146/1/012002
- PÁSSARO, J. P. A. (2022). NUMERICAL DEVELOPMENT AND OPTIMIZATION OF THERMAL STORAGE SYSTEMS BY PHASE CHANGE. DOCTORATE IN MECHANICAL ENGINEERING. http://hdl.handle.net/10362/150113
- Rahmat, M. A. A., Abd Hamid, A. S., Lu, Y., Ishak, M. A. A., Suheel, S. Z., Fazlizan, A., & Ibrahim, A. (2022). An Analysis of Renewable Energy Technology Integration Investments in Malaysia Using HOMER Pro. *Sustainability*, 14(20), 13684. https://doi.org/10.3390/su142013684

- Rani, P., & Tripathy, P. P. (2023). CFD coupled heat and mass transfer simulation of pineapple drying process using mixed-mode solar dryers integrated with flat plate and finned collector. *Renewable Energy*, 217. https://doi.org/10.1016/j.renene.2023.119210
- Selimefendigil, F., Okulu, D., & Öztop, H. F. (2023). Photovoltaic Thermal Management by Combined Utilization of Thermoelectric Generator and Power-Law-Nanofluid-Assisted Cooling Channel. *Sustainability*, 15(6). https://doi.org/10.3390/su15065424
- Shamshiri, R. R., Sturm, B., Weltzien, C., Fulton, J., Khosla, R., Schirrmann, M., Raut, S., Basavegowda, D. H., Yamin, M., & Hameed, I. A. (2024). Digitalization of agriculture for sustainable crop production: a use-case review. *Frontiers in Environmental Science*, 12. https://doi.org/10.3389/fenvs.2024.1375193
- Suherman, S., Susanto, E. E., Ayu, A. D., & Dea, S. (2021). Experimental investigation of ginger drying using hybrid solar dryer. *Journal of Applied Science and Engineering*, 24(4), 553-564. https://doi.org/10.6180/jase.202108 24(4).0011
- Szpicer, A., Bińkowska, W., Wojtasik-Kalinowska, I., Salih, S. M., & Półtorak, A. (2023). Application of computational fluid dynamics simulations in food industry. European Food Research and Technology, 249(6), 1411-1430. https://doi.org/10.1007/s00217-023-04231-y
- Tome, U., Nosan, S., Vidrih, B., Bogić, S., Navickaite, K., Vozel, K., Bobič, M., & Kitanovski, A. (2024). Small demonstrator of a thermoelectric heat-pump booster for an ultra-low-temperature district-heating substation. *Applied Energy*, 361. https://doi.org/10.1016/j.apenergy.2024.122899
- Wan, H., Shen, B., Gluesenkamp, K., & Li, Z. (2023, 5/15/2023). Modelling and Simulation of a Thermoelectric Heat Pump with Micro-Channel Heat Transfer Conference: 14th IEA Heat Pump Conference Chicago, Illinois, United States of America 5/15/2023 8:00:00 AM-5/18/2023 8:00:00 AM, United States. https://www.osti.gov/biblio/1976032
- Wang, P., Liu, G., Ao, S., Sun, D., Yu, B., & Wu, X. (2021). Numerical investigation of airflow and heat transfer characteristics and optimal design of the American ginseng drying room. Applied Thermal Engineering, 183. https://doi.org/10.1016/j.applthermaleng.2020.115885
- Workineh Daksa, T., & Neme Tolesa, G. (2023). Review the Design of the Solar Dryer for the Dryer of Fruit and Vegetable Dryers. *International Journal of Food Engineering and Technology*. https://doi.org/10.11648/j.ijfet.20230701.11
- Xu, Q., Deng, B., Wang, Y., Liu, W., & Chen, G. (2023). Small, affordable, ultra-low-temperature vapor-compression and thermoelectric hybrid freezer for clinical applications. *Cell Reports Physical Science*, 4(12). https://doi.org/10.1016/j.xcrp.2023.101735
- Zeinab, R., Hamid, M., Mehran, A., & Hamid-Reza, A. (2022). Configuration Designs and Recent Applications of Photovoltaic-Thermal Solar Collectors for Drying Agricultural Material: A Review. Biomechanism and Bioenergy Research, 1(1), 34-46. https://doi.org/10.22103/bbr.2022.18904.1002